ELSEVIER

Journal of Alloys and Compounds 434–435 (2007) 572–576

Journal of ALLOYS AND COMPOUNDS

www.elsevier.com/locate/jallcom

Medium-ranged interactions of transition-metal (3d and 4d) impurity pairs in Al and atomic structures of Al-rich Al–transition-metal alloys

T. Hoshino [a,*], N. Fujima [a], M. Asato [b], R. Tamura [a]

[a] *Department of Applied Physics, Faculty of Engineering, Shizuoka University, Hamamatsu 432-8561, Japan*
[b] *Department of General Education, Tokyo Metropolitan College of Technology, Shinagawa-ku, Tokyo 140-0011, Japan*

Available online 28 September 2006

Abstract

We give systematic *ab initio* calculations for the interaction energies (from first to eighth neighbors) of impurity pairs X–X (X = Sc–Zn, Y–Cd) in Al and discuss the micromechanism of the structural stability of Al-rich AlX alloys. The calculations are based on the generalized gradient approximation in the density-functional theory and employ the all-electron full-potential Korringa–Kohn–Rostoker Green's function method for point defects, which guarantees the correct embedding of the cluster of impurities and vacancies in an otherwise perfect crystal. We show: (1) the fundamental features of phase diagrams of these alloys, such as ordering and segregation, are understood by the sign of first-neighboring X–X interaction energies; (2) the structural stability of Al-rich AlX alloys such as $L1_2$ (Al_3Sc and Al_3Y), DO_{22} (Al_3V and Al_3Nb), and Mackay icosahedron in AlMn quasicrystal, are understood qualitatively by using the medium-ranged and oscillating X–X interactions, due to the strong sp-d (Al–X) hybridization; (3) the strength and oscillating behavior of the medium-ranged X–X interaction energies are specified very well by the d-electron numbers of X impurities.

Keywords: Full-potential KKR; Medium-ranged X–X interaction; sp-d Hybridization; Many-body interaction; Generalized-gradient approximation in density-functional theory

1. Introduction

Al-rich alloys with transition metals (Sc–Ni, Y–Pd), being important because of the desirable technological properties of many of these alloys, form a variety of atomic structures depending on d-electron number (n_d) [1]: for example, $L1_2$ for Al_3Sc and Al_3Y ($n_d = 1.4$–1.6), DO_{22} for Al_3V and Al_3Nb ($n_d = 3.3$–3.7), and the Mackay icosahedron (MI, $Al_{42}Mn_{12}$ with a vacancy at the center) in the metastable quasicrystal (QC) phase for $Al_{80}Mn_{20}$ ($n_d \sim 5.9$)[2–4]: the numbers of n_d are the values obtained by the calculations for single X impurities in Al. It was also shown by many experiments on precipitation strengthening that the mechanical strength of the $Al_{1-c}X_c$ (X = Cu, Zn; $c < 0.05$) changes very much by the insertion of the other elements, for example Mg, and is correlated strongly to the atomic structures of small clusters at the initial stage of the Guinier–Preston (GP) zone formation [5–9]. We have already studied systematically the interactions characteristic to the Al-rich AlX (X = Sc–Zn, Y–Cd) alloys, such as the first-neighboring (1st-NEI) X–X (X = Na, Mg, Si, Sc–Zn, Y–Sn) interaction energies (IEs) in Al [7] and the solution energies of X (X = Na, Mg, Si, Sc–Zn, Zr–Ag) in Al [8], and have shown that the Al–X (X = 3d and 4d) metallic bonding, due to the sp-d (Al–X) hybridization, are very much stronger than the d–d (X–X) bonding in Al. This strong sp-d metallic bonding is an important characteristic feature of X (=3d and 4d) in Al, being very different from the sp-d (Cu–X (X = 3d) and Ag–X (X = 4d)) metallic bonding in Cu and Ag where the d–d (X–X) bonding is much stronger than the sp-d (Cu–X and Ag–X) metallic bonding: it is noted that the strength of sp-d hybridization is correlated to the sp-electron numbers of metallic hosts (3 for Al, and 1 for Cu and Ag). As a result, the 1st-NEI X–X interactions are strongly repulsive in Al, while strongly attractive in Cu and Ag: these results agree with the experimental phase diagrams (ordering for AlX alloys and segregation for CuX and AgX alloys) [10]. We also quantitatively studied the characteristic feature of Al-host: the total energy differences among fcc, hcp, and bcc structures are very small and the Wigner–Seitz radius dependence of total energies is almost the same for these structures [6]. These results show that the high-density sp-electrons of Al are

* Corresponding author. Fax: +81 53 478 1276.
E-mail address: tsthosh@ipc.shizuoka.ac.jp (T. Hoshino).

0925-8388/$ – see front matter © 2006 Elsevier B.V. All rights reserved.
doi:10.1016/j.jallcom.2006.08.191

strongly free-electron-like and that the atomic rearrangements of Al atoms occur easily on condition that the total electron densities do no change very much (weak structure dependence). The smallness of vacancy formation energy in Al also confirms the free-electron-like character of sp electrons of Al because the very small vacancy formation energy is due to the strong screening effect of free-electrons-like electrons, as discussed in Ref. [6]. Thus, we may expect that the atomic structures of Al-rich AlX (X = 3d and 4d) alloys are mainly determined by the medium-ranged X–X interactions beyond the first-neighbor distance [11,12]: it is noted that X atoms are not located at the first-neighor sites because of the strong repulsion at first-neighbor distance.

We have also shown that the cluster expansion converges rapidly for the binding energies of large agglomerates of vacancies and X (=Cu, Zn, Mg) impurities in Al [6,9]. For example, the binding energy of 13 vacancies (or 13 X impurities), consisting of a central and its 12 neighbors, is reproduced within the error of ∼0.005 eV per vacancy (or impurity atom), if the pair interactions up to the fourth-neighbor and many-body IEs among first-neighbors, up to the four-body terms, are taken into account in the cluster expansion. It is noted that the many-body IEs among far-neighbors (including up to fourth-neighbor) beyond first-neighbor distance may be neglected for these impurities and vacancies [9]. We have also found that the shapes of GP zones of Cu and Zn in $Al_{1-c}X_c$ (X = Cu, Zn; $c < 0.05$) alloys are understood by the sign and magnitude of three-body (triangle) IEs among first-neighbors, just as the sign and magnitude of the 1st-NEI two-body IEs are connected with the different type of phase diagrams of binary alloys, such as segregation, solid solution, and ordering [13]. The three-body (triangle) IEs of Cu impurities and Zn impurities are, respectively, positive (0.03 eV, repulsion) and zero, which correspond to the (0 0 1) disk and the spherical shape of the GP zones: it is noted that there is no triangle cluster of first-neighbors in the (0 0 1) layer of fcc structure.

In the present paper we give systematic calculations for X–X (X = 3d and 4d elements) IEs in Al and discuss: (1) the X–X interactions due to the sp-d hybridization are strong and medium-ranged, and their energies show the oscillating behavior for the interatomic distance; (2) the atomic structures of Al-rich AlX alloys such as $L1_2$ (Al_3Sc and Al_3Y), DO_{22} (Al_3V and Al_3Nb), and MI in AlMn QC, may be understood by the X–X interactions; (3) the strength and oscillating behavior of X–X interactions are specified very well by the d-electron numbers of single X impurities in Al.

2. Method of calculations

All the calculations are based on the generalized gradient approximation in the density-functional theory [14]. In order to solve the Kohn–Sham equations, we use multiple-scattering theory in the form of the KKR Green's-function method for full potentials (FP) for perfect metals and defect systems. The advantage of the Green's function method is that, by introducing the host-Green's function, the embedding of point defects in otherwise ideal crystal is described correctly, differently from the usual supercell or cluster calculations. At present we can treat the point defects in complex periodic systems because the host-Green's functions for complex periodic systems are calculated by the screened FPKKR method [15–17]. It is noted that the present cluster expansion [6,9] is different from that proposed by Connolly–Williams approach [18] where the two-body and many-body IEs are determined by fitting to the total energy differences among ordered alloys. Thus, in case of Connolly–Williams approach, the two-body and many-body IEs depend on the set of ordered alloys, which is chosen appropriately. The present approach, while restricted to the dilute limit, considers only atomic configurations, the energy differences of which define uniquely the two-body and many-body IEs [9]. For the low-concentration alloys, the concentration dependence of two-body and many-body IEs may be accurately calculated by the present method combined with the direct configurational averaging [19].

3. Calculated results

In the next three paragraphs we discuss the following. First we review the important points of the experimental results for the atomic structures of Al-rich AlX (X = Sc, V, Mn). Next, we give and discuss the calculated results for the X–X (X = Sc–Zn, Y–Cd) IEs in Al. Subsequently we show that the structural stability of Al-rich AlX (X = Sc, V, Mn, Y, Nb) alloys are understood very well by the present results for X–X IEs. It is also shown that the strength and oscillating behavior of X–X interactions, due to the sp-d hybridization, are very well specified by the d-electron number of single X impurities in Al.

Fig. 1 show the atomic structure of $L1_2$ (Al_3Sc, Al_3Y), DO_{22}(Al_3V, Al_3Nb), and the MI in $Al_{80}Mn_{20}$ QC [1–4]. For $L1_2$ structure, X atoms are located at the second-neighbor distance, and for DO_{22} structure some part of X atoms are located on the third-neighbor distance. For the MI in AlMn QC, the experimental value of the 1st-NEI Mn–Mn distance may be ∼4.9 Å [2], corresponding to the third-neighbor distance in fcc (0–3 in Fig. 1(b)).

Fig. 2 show the calculated results for the pair, triangle, and tetrahedron IEs of 1st-NEI X impurities in Al. Positive values mean repulsion, while negative ones attraction. The calculated results are summarized as follows:

(1) The two-body and many-body IEs of 3d impurities are almost the same to those of 4d impurities located at the same column in the periodic table.
(2) The n-body interactions are weaker and weaker with the increase of n.
(3) In most cases the two-body interactions are dominant. Thus, we can explain the difference between segregation and ordering of alloys by using the sign and magnitude of 1st-NEI pair IEs (positive for order and negative for segregation) [11]: the experimental results of AlX alloys show ordered phases for X = Sc–Ni, Y = Pd, while segregation phases for X = Cu, Zn, Ag, and Cd [10]. The chemical trend of two-body IEs is discussed in Ref. [7]. For Cu, the two-body chemical interaction is very weak. Thus, the lattice distor-

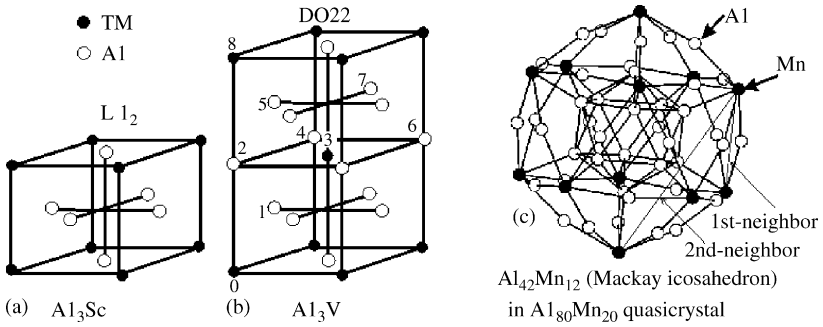

Fig. 1. Atomic structures of Al-rich AlX alloys (X = Sc, V, Mn). The Mackay icosahedron consists of $Al_{42}Mn_{12}$ with a vacancy at the center. The first to eighth neighbors in fcc structure are indicated by the sites 1–8 around a central site 0, shown in (b).

tion effect may be essential for the binding of Cu impurities: it is noted that the atomic-size misfit is large for Cu impurities in Al. We are now studying the lattice distortion effect for agglomerates of Cu impurities in Al [8].

Fig. 3 give the calculated results for X–X (X = Sc–Zn, Y–d) IEs in Al. The d-electron numbers of single X impurities in Al, as well as the deviation from the charge neutrality, are shown in Table 1: all the values are the quantities in the same Wigner–Seitz cell as that of the Al-host atom. We find that the electron numbers of X impurities in Al slightly decrease for the early d-impurities, while slightly increase for the late d-impurities. The main part of these deviation may be understood by considering the differences of atomic-radius of X pure metals with that of Al: the atomic-radii of early d-metals are larger than that of Al, while those of late d-metals smaller [8]. Thus, we may conclude that the deviations from the charge neutrality may be fairy smaller than the values in Table 1: the present results may deny the effective-negative-valence-model by Raynor [20]. The distance-dependence and element-dependence of X–X IEs are summarized as follows:

(1) The interactions are medium-ranged and show the Friedel-type oscillating behavior for the interatomic distance.
(2) The strength and oscillating behavior of IEs are very well specified by the d-electron numbers of single impurities in Al (see Table 1).

In order to confirm the result (2) we calculated the pair IEs of different kinds of impurities (Fig. 4). It is noted that the strength and oscillating behavior of IEs of Y–Z (for example, Y = Ti and Z = Cr) are almost the same, at least at the distances larger than the third-neighor, to that of the IEs of X–X (for example X = V) with the average d-electron number of X and Y

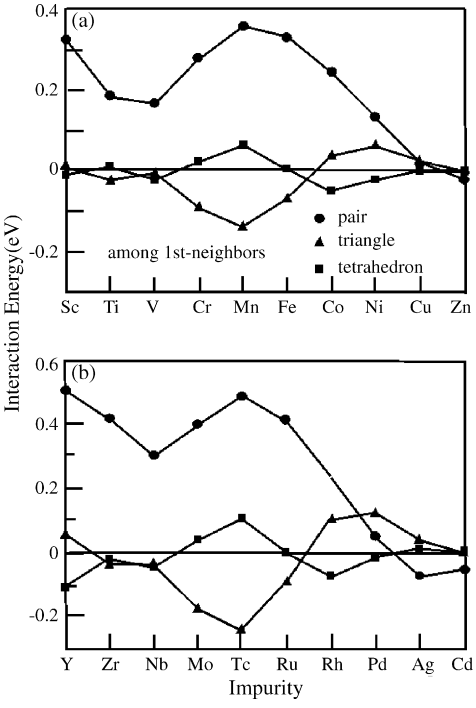

Fig. 2. Pair, triangle, and tetrahedron interaction energies of first-neighboring X ((a) X = Sc–Zn; (b) X = Y–Cd) impurities in Al.

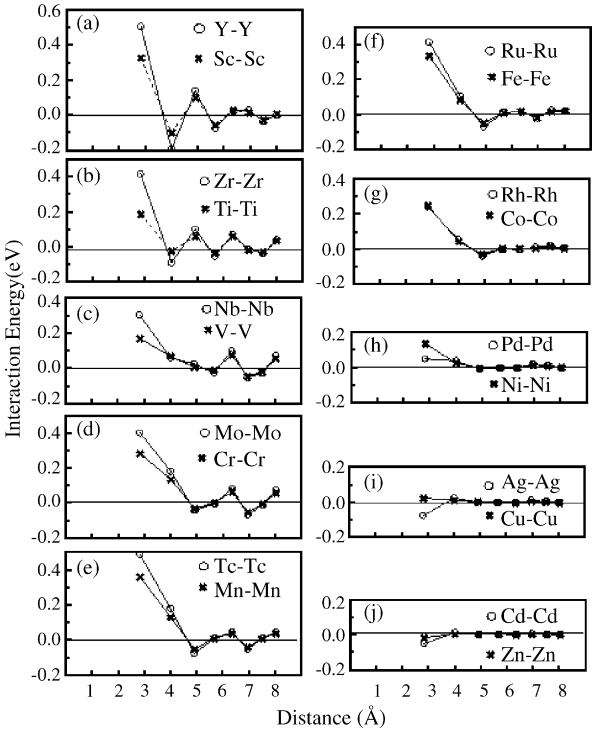

Fig. 3. Distance dependence (first to eighth in Fig. 1(b)) of interaction energies between two equal impurities in Al and results of 3d and 4d impurities of the same column in the periodic table.

Table 1
Deviation from charge neutrality (ΔQ) and d-electron numbers (n_d) of X impurities in Al

Sc	Ti	V	Cr	Mn	Fe	Co	Ni	Cu	Y	Zr	Nb	Mo	Tc	Ru	Rh	Pd	Ag
ΔQ																	
−0.39	−0.25	−0.06	0.12	0.27	0.39	0.47	0.51	0.47	−0.75	−0.71	−0.61	−0.3	−0.15	0.05	0.18	0.24	0.16
n_d																	
1.6	2.6	3.7	4.8	5.9	7.0	8.0	8.9	9.7	1.4	2.4	3.3	4.5	5.7	6.8	7.9	8.8	9.5

Both quantities are the values in the same Wigner–Seitz cell as that of the Al-host atom.

(Fig. 4(a)). This result confirms that the oscillating behavior of the medium-ranged X–X interactions are due to the strong the sp-d hybridization: the phase shift of sp-electron waves of Al may be obtained by the calculations of single X transition-metal impurities in Al and, as a result, may be a function of the d-electron numbers of single X impurities. Their strength may also be a function of d-electron numbers. For the 1st-NEI pairs the direct d–d interaction also become important. The details will be published elsewhere [21].

We now discuss the structural stability of atomic structures of Al-rich AlX (X = Sc, V, Mn, Y, Nb) alloys, such as $L1_2$ for Al_3Sc and Al_3Y, DO_{22} for Al_3V and Al_3Nb, and MI ($Al_{42}Mn_{12}$) in the AlMn QC. For Sc and Y, the X–X interaction is strongly repulsive for the 1st-NEI pairs, strongly attractive (negative and large) for the second-neighbor pairs, and repulsive for the third-neighbor pairs (Fig. 3(a)). Thus, we can easily expect that Sc and Y atoms are arranged at the interval of the second-neighbor interatomic distance (corresponding to $L1_2$ in Fig. 1(a)). For V and Nb, the interaction is strongly repulsive for the second-neighbor pairs and very weak around the third-neighbor pairs (Fig. 3(c)). Thus, for Al_3V and Al_3Nb the DO_{22} structure (Fig. 1(b)) may become stable compared with the $L1_2$ structure. For X = Cr, Mn, and Fe (Mo, Tc, and Ru), as seen in Fig. 3(d)–(f), the interactions are very repulsive up to the distance being just a little bit shorter than the third-neighbor distance and become very attractive around the third-neighbor distance (4.7–5.0 Å): for Mn the strongest attraction (−0.05 eV) at 4.9 Å. Thus, it is obvious that Mn atoms prefer to be arranged at the interval of the interatomic distance between 4.7 and 5.0Å. We can easily expect that the atomic structure of a locally high-symmetric icosahedron of 12 Mn impurities, being a sublattice of MI (see Fig. 1(c)), may be very stable because it includes a large number (30) of Mn–Mn pairs at the distance of ∼4.9 Å: for this atomic structure the energy gain due to the Mn–Mn interactions is as large as ∼−1.5 eV (=−0.0.5 × 30). It is noted that this interatomic distance (4.7–5.0 A) is very close to one of the observed interatomic distances (4.7–4.9 and ∼7.5 Å) of Mn–Mn pairs [2], although the present calculated interatomic distance of Mn–Mn pairs may be changed a little bit by the quantitative calculations based on the atomistic simulations, as mentioned in the last section. We also found that the calculated results with spin-polarization effect don't change very much the present results for Cr, Mn, and Fe, although the Mn–Mn interaction at ∼7.5 Å, corresponding to the second-neighbor of a sublattice icosahedron of Mn_{12}, may change from the weak repulsion to the weak attraction (stability of MI) by the inclusion of magnetism. The details, including the discussion for the effect of a vacancy at center of MI, will be discussed elsewhere [21].

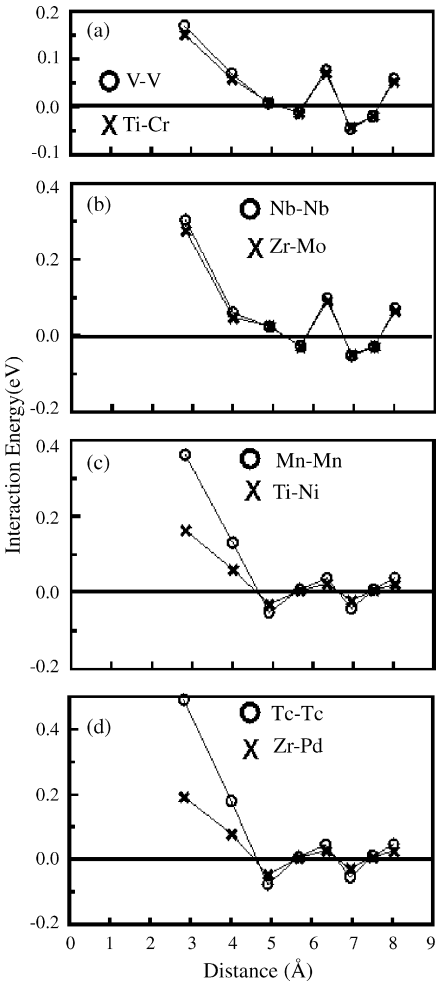

Fig. 4. Distance dependence (first to eighth in Fig. 1(b)) of interaction energies between two different kinds of impurities. See text for details.

4. Conclusions

We have qualitatively shown that the structural stability of the MI in AlMn QC, as well as $L1_2$ and DO_{22} structures of the Al-rich AlX (X = Sc, V, Y, Nb) alloys, are understood by the medium-ranged X–X interactions due to the strong sp-d (Al–X) hybridization in Al. In order to confirm quantitatively the present mechanism of the structural stability of MI, we plan to perform the atomistic simulations [22] with the accurate embedded-atom-method-potentials (EAMP), all the parameters in which are determined by fitting to the *ab initio* input data,

obtained from the present calculations, following the way of Ref. [23]. We believe that the inclusion of the strong IE of Mn with the neighboring Al atoms and the medium-ranged Mn–Mn IEs, discussed in the present paper, is essential for the construction of EAMP of AlMn QC.

References

[1] F. Mondolf, Aluminium Alloys: Structure and Properties, Butterworths, Boston, 1976.
[2] M. Maret, A. Pasturel, C. Senillou, J.M. Dubois, P. Chieux, J. Phys. France 50 (1989) 295.
[3] V. Elser, C.L. Henley, Phys. Rev. Lett. 55 (1985) 2883.
[4] P.A. Bancel, P.A. Heiney, Phys. Rev. B33 (1986) 7917.
[5] T. Sato, S. Hirosawa, K. Hirose, T. Maeguchi, Metall. Mater. Trans. 34A (2003) 2745.
[6] T. Hoshino, M. Asato, R. Zeller, P.H. Dederichs, Phys. Rev. B70 (2004) 094118.
[7] T. Hoshino, F. Nakamura, Metastable Nanocryst. Mater. 24–25 (2005) 237.
[8] T. Hoshino, M. Asato, N. Fujima, N. Papanikolaou, Trans. Mater. Res. Soc. Jpn. 30 (3) (2005) 877.
[9] F. Nakamura, T. Hoshino, S. Tanaka, K. Hirose, S. Hirosawa, T. Sato, Trans. Mater. Res. Soc. Jpn. 30 (3) (2005) 873.
[10] T.B. Massalski, Binary Alloy Phase Diagrams, 2nd ed., ASM International, New York, 1990.
[11] J. Friedel, Helv. Phys. Acta Sci. (Paris) 305 (1987) 171.
[12] J. Zou, A.E. Carlsson, Phys. Rev. Lett. 70 (1993) 3748.
[13] M. Asato, T. Mizuno, T. Hoshino, H. Sawada, Mater. Trans. 42 (2001) 2216.
[14] T. Hoshino, T. Mizuno, M. Asato, H. Fukushima, Mater. Trans. 42 (2001) 2206.
[15] R. Zeller, Phys. Rev. B55 (1997) 9400.
[16] T. Hoshino, M. Asato, T. Nakamura, R. Zeller, P.H. Dederichs, J. Magn. Magn. Mater. 272–276 (2004) e229.
[17] T. Hoshino, M. Asato, T. Nakamura, R. Zeller, P.H. Dederichs, J. Magn. Magn. Mater. 272–276 (2004) e231.
[18] J.W. Connolly, A.R. Williams, Phys. Rev. B. 27 (1983) 5169.
[19] M. Asato, T. Hoshino, J. Magn. Magn. Mater. 272–276 (2004) 1372.
[20] G.V. Raynor, Prog. Met. Phys. 1 (1949) 1.
[21] T. Hoshino, et al., in preparation.
[22] S. Ogata, F. Shimizu, J. Li, M. Wakeda, Y. Shibutani, Proceedings of the BMG-IV Conference, Tennessee, Intermetallics 14 (2006) 1033.
[23] Y. Mishin, M.J. Mehl, D.A. Papaconstantpoulos, A.F. Voter, J.D. Kress, Phys. Rev. B63 (2001) 224106.